Chemical Science

Accepted Manuscript

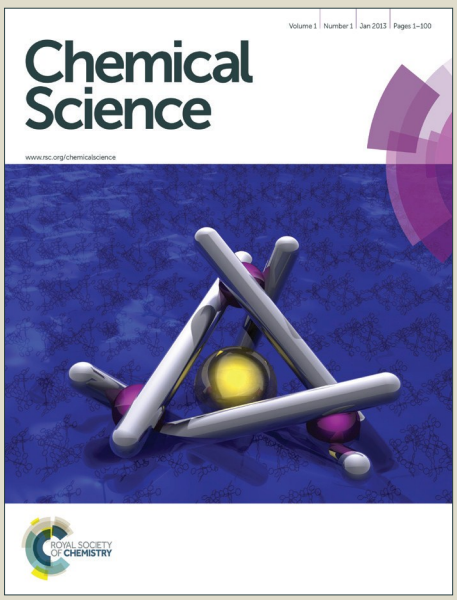

ROYAL SOCIETY OF CHEMISTRY

www.rsc.org/chemicalscience

Chemical Science

EDGE ARTICLE

Ultra large optical modulation of electrochromic porous WO_3 film and the local monitoring of redox activity†

Received 00th January 20xx,
Accepted 00th January 20xx

DOI: 10.1039/x0xx00000x

www.rsc.org/

Guofa Cai, Mengqi Cui, Vipin Kumar, Peter Darmawan, Jiangxin Wang, Xu Wang, Alice Lee-Sie Eh, Kai Qian, and Pooi See Lee*

Porous WO_3 films with ultra–high transmittance modulation were successfully fabricated on different substrates by a novel, facile and economical pulsed electrochemical deposited method with 1.1 s interval time between each pulse. The near ideal optical modulation (97.7% at 633 nm), fast switching speed (6 and 2.7 s), high coloration efficiency (118.3 $cm^2 C^{-1}$), and excellent cycling stability are achieved by the porous WO_3 on ITO–coated glass. The outstanding electrochromic performances of the porous WO_3 film were mainly attributed to the porous structure, which facilitates the charge-transfer, promotes the electrolyte infiltration and alleviates the expansion of the WO_3 during H^+ insertion compare to that of the compact structure. In addition, the relationships between structural and electrochemical activity of the electrochromic WO_3 films were further explored by the Scanning Electrochemical Microscopy. These results testify that the porous structure can promote the infiltration of electrolyte and reduce the diffuse path, which consequently enhance the electrochemical activity.

1. Introduction

The decreasing availability of fossil fuels leads to the exploitation of renewable energy resource.[1-3] The fraction of the world's primary energy mainly used for heating, cooling, ventilation, and appliances in buildings reaches as much as 30–40%.[4] Therefore, materials which are capable of converting and saving renewable energy in buildings are desirable. Electrochromic materials can reversible change their optical properties such as transmittance, reflectance and absorptance by the application of a small electric field, which is highly attractive for a wide range of potential applications, such as energy efficient smart windows, large area information displays and antiglare automotive mirrors.[5-9] Smart glass windows based on electrochromics are regarded as very promising means of converting and saving renewable energy due to their high chromatic contrast, low cost and environmentally friendly, which reduced electricity consumption for cooling and decreased lighting costs by about 50% in addition to a lowered peak electricity power demand by up to 16% for commercial buildings.[4]

Tungsten trioxide (WO_3) has been extensively investigated and identified as one of the most promising inorganic electrochromic materials.[10, 11] However, unsatisfactory optical modulation, long switching time and short life time limit its electrochromics effectiveness. The ideal optical modulation of electrochromic material is 100%, that is the material is fully transparent on the bleached state and fully opaque on the colored state. To date, only a few of research groups have reported the optical modulation of WO_3 material over 80%. Yang et al.[12] reported ultrathin WO_3 film exhibiting optical modulation of 76.2% at 633 nm. Cong et al.[13] demonstrated the optical modulation of single–crystalline WO_3 quantum dots can reach to 85% at 633 nm, but the experimental process is complex and the yield of the product is low. Recently, Liu et al.[14] reported the WO_3 crystalline nanoparticles film prepared by "nano to nano" electrodeposition approach has optical modulation of 92% at 633 nm, the experimental process involved a complex two–step fabrication procedure and the switching time of the film is 9 s for coloring and 15 s for bleaching. The electrochromic phenomenon of metal oxide is attributed to the injection/extraction of electrons and ions.[15-17] Nano–architectures are gaining importance in various electrochemical device applications. The nanostructures of the intercalation compound not only facilitated the electrolyte penetration and shorten the ionic diffusion paths within the electrochromic materials, but also alleviated the expansion and contraction of the host material during guest insertion and extraction. Up to now, lots of methods have been applied to prepare the nanostructured WO_3 films, such as hot–filament assisted synthesis[18] sol–gel[19], sputtering[20], hydrothermal[21], solvothermal[22] and electrodeposition processing[23]. Among these physical and chemical fabrication techniques, electrochemical deposition methods are of particular interest due to their low cost, feasibility for large area film growth and without further thermal treatment. In addition, various

School of Materials Science and Engineering, Nanyang Technological University, 50 Nanyang Avenue, Singapore 639798, Singapore
† E-mail: pslee@ntu.edu.sg, Homepage: http://www.ntu.edu.sg/home/pslee/
†Electronic Supplementary Information (ESI) available: See DOI: 10.1039/x0xx00000x

conductive substrates can be used with this deposition technique, such as conductive glass and flexible or stretchable conductive polymer substrates. Especially, flexible substrates have recently attracted great interest due to portable and highly integrated devices which needs to be small size, lightweight, and compliant on highly flexible substrate.[24-26] Continuous and pulsed electrochemical deposited WO_3 films have been demonstrated using deposition solutions prepared by dissolving the sodium tungstate in diluted acid or tungsten powder in hydrogen peroxide (H_2O_2).[27-29] However, none of these WO_3 film exhibit satisfying electrochromic performance. Therefore, it is of great importance to unravel the interdependence of desirable electrochromic behavior and materials structures.

In the past, electrochemical characterizations for electrochromic material are mostly done on macroscopic or device level, which provide the average measurement across the interfaces. However, localized studies on the charge transport process and on electrochemical reaction are less investigated.[30, 31] A deeper understanding of local electrochemical properties of electrochromic material will be beneficial to establish relationships between structural design and electrochemical activity for enhanced electrochromic performance. Scanning electrochemical microscopy (SECM) has been very successful in this respect and used for providing insightful electrochemical characterization on sub–micrometer scale investigation of a wide range of materials and interfaces.[32, 33] We have previously introduced SECM measurements to probe the localized interfacial kinetics at the interface of electrolyte/electrode and extract the effective heterogeneous charge transfer rate constant based on polyaniline and MnO_2 for supercapacitor application.[34, 35]

Herein, one novel, facile and economical pulsed electrochemical deposition with defined interval time between each pulse for porous WO_3 film deposition is demonstrated. The porous WO_3 films were fabricated on different conductive substrates without any template and no further thermal treatment is required. Electrochemical and electrochromic properties of the porous WO_3 film were evaluated in this paper. The porous WO_3 film exhibits excellent electrochromic performance, including near theoretical optical modulation, fast switching speed, high coloration efficiency and good cycling stability. In addition, the localized charge transport process and electrochemical reaction were investigated by in situ SECM technique to provide in–depth insights on the relationship between microcosmic structural and macroscopic electrochromic performance.

2. Experimental

2.1 Chemicals.

Sodium tungstate dihydrate ($Na_2WO_4{\cdot}2H_2O$, ≥99%) and perchloric acid ($HClO_4$, 70%) were purchased from Sigma–Aldrich. H_2O_2 (30%) was obtained from VWR International Ltd. All the chemicals were used without further purification and all aqueous solutions were prepared from deionized water (Milli–Q, Millipore Corp).

2.2 Preparation of porous WO_3 film.

The deposition electrolyte solution was prepared by dissolving 1.03 g $Na_2WO_4{\cdot}2H_2O$ in 250 ml deionized water, and then 2 ml perchloric acid and 0.65 ml H_2O_2 was added to the above solution under magnetic stirring. Indium tin oxide (ITO)–coated glass, fluorine–doped tin oxide (FTO)–coated glass and ITO–coated polyethylene terephthalate (PET) were used as transparent electrodes. These electrodes were first cleaned with deionized water and ethanol, and then were treated by argon plasma. The pulsed electrodeposition with 1.1 s interval time between each pulse was performed with a Solartron 1470E electrochemical workstation (Farnborough, U.K.) at room temperature using a conventional three–electrode system. The counter electrode was a 2×2 cm^2 platinum foil and the reference electrode was an Ag/AgCl electrode. Pulsed voltages were switched between –0.7 to 0 V. Square waveform pulses were applied with a duty cycle length of 0.2 s. For one deposition cycle, a square waveform pulse at –0.7 V was first applied onto the cell for 0.1 s, followed by another square waveform pulse at 0 V was applied to the cell for 0.1 s. Between each deposition cycle, there is a pause of 1.1s. A whole deposition procedure involves 6000 cycles, with a total deposition time around 7800 s. After deposition, the films were thoroughly washed with methanol and water and finally dried in air. For comparison, WO_3 films on ITO–glass substrates deposited by continuous electrodeposition and pulse deposition with no interval pause time were also prepared.

2.3 Sample characteristics.

The morphology, structure and composition of the WO_3 films are characterized by scanning electron microscopy (SEM, JEOL 7600F, Tokyo, Japan), transmission electron microscope (TEM, JEOL 2010), and X–ray diffraction (XRD, Shimadzu diffractometer with CuKα–radiation (λ = 1.5406 Å)). The Renishaw Raman Microscopy is used to identify Raman spectra conducted using with a charge coupled device array detector at 532 nm laser line. The Raman signals were dispersed by 2400 line mm^{-1} gratings with frequency resolution of ~0.8 cm^{-1} and collected by a Leica 100 × objective lens (NA = 0.85). The surface analysis of the sample has been carried out using the VG ESCALab 220i–XL Imaging X-ray photoelectron spectroscopy (XPS) last calibrated in Sep 2014. Monochromatic Al Kα X–ray (*hv*=1486.7 eV) was employed using a large area lens mode for analysis with photoelectron take–off angle of 90° with respect to surface plane. The maximum analysis depth lay in the range of 4–8 nm. The charge correction is based on C1s in adventitious carbon at 285.0 eV. For chemical state analysis, a spectral deconvolution was performed by a curve–fitting procedure based on Lorentzians broadened by Gaussian using the manufacturer's standard software. The error of binding energy is estimated to be within ± 0.2 eV.

2.4 Electrochemical Characterization.

The electrochemical and electrochromic measurements were conducted in a three–electrode electrochemical cell containing 0.5 M H_2SO_4 aqueous solution as the electrolyte. The voltage supply was from Solartron 1470E. The transmission spectra of WO_3 films under different potential were measured in situ

over the wavelength range from 300 to 900 nm by combination of a SHIMADZU UV–3600 spectrophotometer and Solartron 1470E electrochemical workstation. The test WO_3 films were used as working electrode, Ag wire was used as the reference electrode and a Pt wire was used as the counter electrode. The transmittance of the conductive substrates in the electrolyte was considered to be 100 % and was used as the baseline. Cyclic voltammograms (CVs) and electrochemical impedance spectrum (EIS) tests were also conducted on Solartron 1470 with Ag/AgCl as the reference electrode in both electrochemical measurements. SECM studies were performed on a home built instrument running with the xyz–positioning system and bipotentiostat (Sensolytics GmbH, Germany) in a four electrode configuration with a Pt microelectrode as working electrode 1 (WE1, r_T = 12.5 µm, RG= r_{glass} / r_T = 7, (r_{glass} and r_T are the radius of the glass sheath and the WE1, respectively), the WO_3 film as WE2, a Pt wire as auxiliary electrode, and an Ag/AgCl reference electrode. All electrodes were immersed into 1 mM $[Ru(NH_3)_6]Cl_3$ in 0.1 M KCl. SECM feedback mode approach curves were acquired through SECMx software. The WE1 current and WE1–WO_3 distance during the approach curve measurements were normalized to the steady state current and the WE1 radius, respectively using $I_T = i_T/i_{T,\infty}$ and $L = d/r_T$, where i_T and $i_{T,\infty}$ are the probe current and the probe current measured far from the substrate, and d refers to tip-substrate separation distance in SECM. The normalized approach curves I_T vs. L were then fitted to the analytical approximation of Cornut and Lefrou[36] to obtain the normalized heterogeneous rate constant κ.

3. Results and discussion

3.1 Microstructure characteristics

The current-time responses and corresponding SEM images of the WO_3 film on ITO–coated glass are shown in Fig. 1. Uniform granules and compact smooth surface are observed in the films prepared by continuous and pulsed electrodeposition without interval time as shown in Fig. 1b and d, which are similar to that reported by previous literatures.[27-29] The size of the granules prepared by continuous electrodeposition is about 15 nm, but the size of the granules formed by no interval time pulsed electrodeposition is about 30 nm, which is larger than that of the continuous electrodeposition. However, the WO_3 film exhibits porous and nanoscale interconnecting network structure when the interval time 1.1 s was present between each pulse (Fig. 1f). The nanoscale interconnecting network is made up of flaky WO_3 with thicknesses of about 25 nm. It is worth noting that during the interval pause time, the deposition cell was under a positive open circuit potential of 0.63 V (Fig. 1e). The mechanism of the electrodeposition can be illustrated as follows: the dimeric peroxy–tungstate $[(O_2)_2W(O)\cdot O\cdot W(O)(O_2)_2]^{2-}$ ($^{W_2O_{11}^{2-}}$, tungsten is in a +VI oxidation state and (O_2) denotes a peroxide ligand) is formed in deposition electrolytes by dissolving Na_2WO_4 into acidic H_2O_2 solutions, which undergoes a reduction and gives rise to tungsten trioxide and molecular oxygen during the

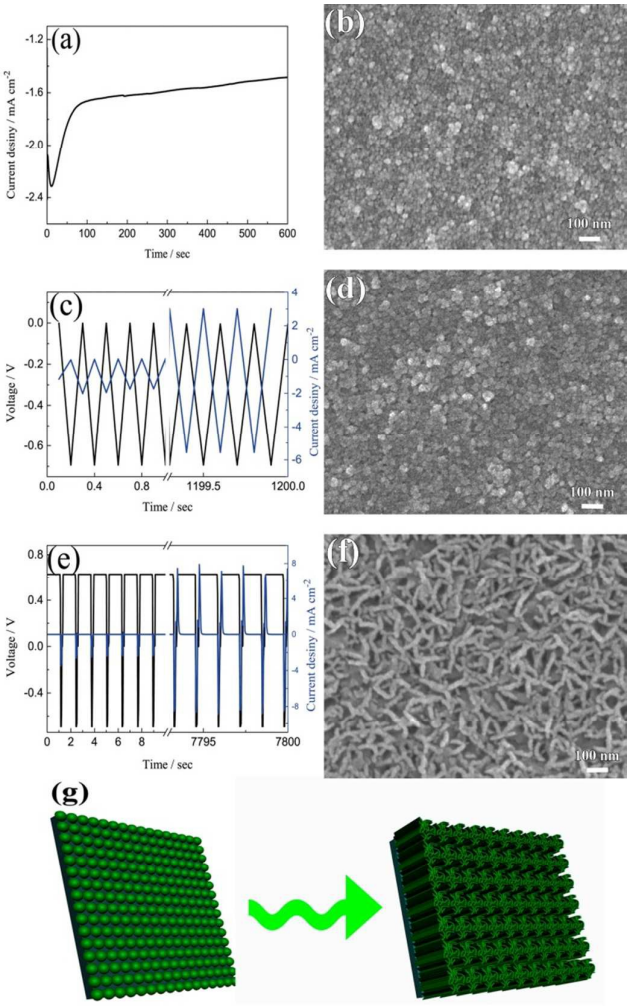

Fig.1 The current-time responses and the corresponding SEM imges for electrodeposited WO_3 films on ITO glasses: (a,b) continuous deposition, (c,d) pulsed electrodeposition without interval time, (e,f) pulsed electrodeposition with 1.1 s interval time between each pulse. (g) the formation process of porous and interconnecting flaky WO_3 film.

electrodeposition procedure.[37, 38] The reaction can be described as follows:

$$2WO_4^{2-} + 4H_2O_2 \rightarrow W_2O_{11}^{2-} + 2OH^- + 3H_2O \quad (1)$$

$$W_2O_{11}^{2-} + (2+3x)H^+ + 3xe^- \rightarrow 2H_xWO_3 + \frac{(2+x)}{2}H_2O + \frac{8-x}{4}O_2 \quad (2)$$

$$H_xWO_3 \rightarrow WO_3 + xH^+ + xe^- \quad (3)$$

The film exhibits blue color during the electrodeposition procedure, which are mainly H_xWO_3 and exhibits metallic properties.[39] The formation H_xWO_3 compound is evident from the gradual increase in current density in Fig. 1(c). The color gradually fades when the open circuit voltage arises to positive potential after electrodeposition and WO_3 is formed. On the basis of the mechanism mentioned above, a model for the electrodeposited WO_3 film is proposed. During the continuous cathodic electrodeposition procedure, due to the uniform

electric field distribution on the surface of the substrates and the electrostatic repulsion between the negative surface charge and the negative ions, the nucleation occurs simultaneously over the entire substrates surface. Therefore, the film prepared by continuous electrodeposition is comprised of small granules. However, H_xWO_3 deposits are nucleated as hemispherical islands on the substrates during the pulsed electrodeposition, and the electric field is locally enhanced by the aspect ratio of the islands. Like a lightning–rod effect, the electric field lines concentrate on the convexity of a lightning conductor.[40, 41] New H_xWO_3 nuclei are formed near the tip by the over potential, hence the size of the granules prepared by pulsed electrodeposition is larger than that of the granules prepared by continuous electrodeposition. When there is an interval time between each pulsed electrodeposition and the open circuit potential is positive during the interval time, the surface of the H_xWO_3 nuclei is charged positively during the interval time. A positive surface charge is preferred for the growth of H_xWO_3 nuclei because of the electrostatic attraction between the positive surface charge and the negative ions. With the combination of positive surface charge and lightning–rod effect, the granules interlace with one another to form a porous flaky structure. Simultaneously, the newly nucleated small islands around the flakes are dissolving under the positive potential and form the porous and nanoscale interconnecting network structure.

The model of the electrodeposition is further confirmed by changing the length of pulsed time and interval time as shown in Fig. S1 and Fig. S2 in Supporting Information. When the fixed interval time was 1.1 s between each pulsed electrodeposition cycle, short nano–chains are observed in the film prepared with an applied duty cycle length of 4 s (Fig. S1a). The nano–chain is made up of small granules and the length is 50~80 nm. The length of the nano–chain is longer when the length of duty cycle decreases to 1 s (Fig. S1b), and some porous and flaky network structure appeared in the film prepared with an applied duty cycle length of 0.5 s (Fig. S1c). When the duty cycle length is fixed for 0.2 s, some flaky structure are observed in the film prepared by applied 0.4 s interval time between each pulsed electrodeposition cycle (Fig. S2a). With increasing the duty cycle length, there is more positive charge gathered on the surface of the working electrode and leads to more flaky structure interconnected with each other (Fig. S2b and c). Therefore, the porous and interconnecting flaky WO_3 film can only be formed by pulsed deposition under shorter duty cycle length and longer interval time. Fig. 1g summarizes the formation process of porous and interconnecting flaky WO_3 film. Moreover, the porous and interconnecting flaky WO_3 film can be deposited not only on the ITO glass, but also on FTO glass and ITO–coated PET flexible substrate as shown in Fig. S3. It illustrates that this method has wide applications on various conductive substrates.

Fig. 2a shows the Raman spectra of the WO_3 films. Typically, all the films exhibit a broad peak centered at 670 cm^{-1} resulting from the W–O stretching vibrations and a relatively sharp peak at 957 cm^{-1} resulting from the W=O stretching mode of terminal oxygen atoms. In addition, there is a weak

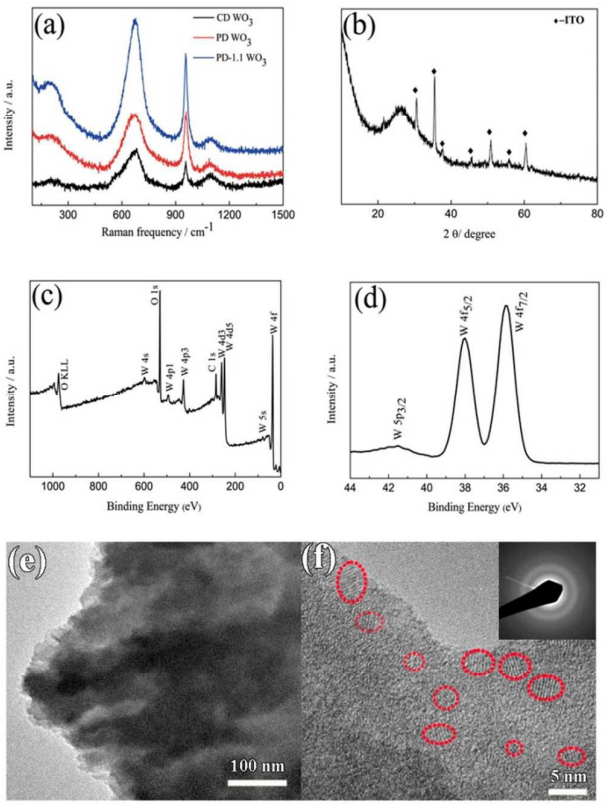

Fig.2 (a) Raman spectra of the WO_3 films, CD WO_3 corresponding to the WO_3 film prepared by continuous deposition, PD WO_3 corresponding to the WO_3 film prepared by pulsed electrodeposition without interval time, PD–1.1 WO_3 corresponding to the WO_3 film prepared by pulsed electrodeposition with 1.1 s interval time between each pulse. (b) XRD pattern of the WO_3 film prepared by continuous deposition. (c, d) XPS surveys spectra and detail of the W4f peak for porous WO_3 film. (e, f) TEM images of the WO_3 scratched from the WO_3 film on ITO substrate prepared by pulsed electrodeposition with 1.1 s interval time between each pulse (SAED pattern presented in inset).

and broad peak at 202 cm^{-1} ascribed to W–O bending vibration. These results match well with those reported in the literature for WO_3.[42-44] Another weaker and broad peak located around 1092 cm^{-1} arise due to the ITO substrate.[45] The XRD pattern of the film on ITO substrates is presented in Fig. 2b. There is only an additional broadened peak display around $2\theta \approx 26.4°$ after subtracting the diffraction peaks of ITO glass, indicating an amorphous WO_3 in presence. The result is in accordance with the previous reports.[46, 47] XPS measurements were performed to further investigate the chemical composition and oxidation state of films. The XPS survey spectra of porous WO_3 film only contains W, O and C as shown in Fig. 2c. Fig. 2d shows the high resolution XPS spectrum of the W4f peak. There are spin–orbit doublets in this spectrum corresponding to $W4f_{7/2}$, $W4f_{5/2}$ and $W5p_{3/2}$ peaks which are located at 35.9 eV, 38.0 eV and 41.5 eV, respectively. These

values are consistent with those reported in the literature for WO_3.[48, 49] In addition, the ratio of O to W is 3.0 as shown in the Table S1 in Supporting Information. It can be reasoned that W in the films is at the highest +VI oxidation state. The structural characteristics of the porous WO_3 film prepared pulsed electrodeposited with 1.1 s interval time between each cycle is further investigated by TEM, as shown in Fig. 2e and f. From the low magnification image, the WO_3 film exhibits flaky structures. HRTEM and selected area electronic diffraction (SAED) results confirm that most of the film exhibits an amorphous structure. However, areas with low–range order in a few nanometers scale are observed in the HRTEM image, manifesting that there are some nanocrystals dispersed in the amorphous matrix. It is well known that the electrochromic performance of inorganic materials is closely related to its degree of crystallization.[50-52] For example, crystalline WO_3 film exhibited inferior electrochromic performance (such as coloration efficiency, optical modulation and switching time) to amorphous one. Nevertheless, the amorphous WO_3 has poorer cyclic stability.[51, 52] Therefore, the formation of WO_3 nanocrystals is anticipated to be an integrated approach to improve the electrochromic performance of the WO_3 films.

3.2 Electrochemical and electrochromic performance evaluations

In order to evaluate the electrochemical and electrochromic performance, the representative compact and porous WO_3 films with thickness of about 480 nm (Fig. S4) prepared by continuous and pulsed electrodeposition with 1.1 s interval time between each pulse were chosen. Fig. 3a shows the CVs of WO_3 films carried out in the potential region of –0.7~1.0 V (vs. Ag/AgCl) at a scan rate of 20 mV s^{-1}. The presence of two waves in both CV curves, named I and II, is attributed to the insertion of two distinct proton species: hydrated H^+ ions

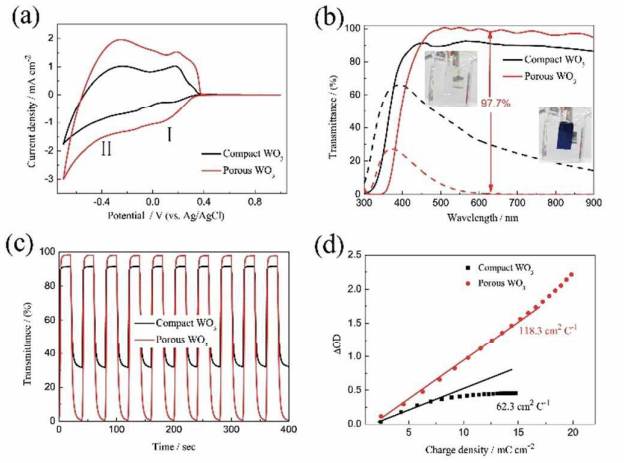

Fig.3 (a) Cyclic voltammograms of WO_3 films on ITO glass as working electrodes in 0.5 M H_2SO_4 at a scan rate of 20 mV s^{-1} in the potential range of –0.7 to 1 V vs. Ag/AgCl. (b) Transmittance spectra of the WO_3 films on ITO glass in the colored (–0.7 V) and bleached (1 V) states between wavelength range of 300 to 900 nm. (c) In situ optical responses of WO_3 films on ITO glass for 20 s per step measured at 633 nm. (d) Optical density variation with respect to the charge density.

absorbed onto WO_3 surface or enclosed into pores of the oxide, and hydrated H^+ ions coming from the bulk solution, respectively.[53] Therefore, the recorded current is due to the H^+ ion intercalation/extraction according to the reaction

$$WO_3 + xH^+ + xe^- \leftrightarrow H_xWO_3 \quad (4)$$

The potentials of redox peaks have no significant difference for both films. However, the cathodic and anodic peak currents of the porous film are much higher than those of the compact film. These indicate that the porous WO_3 film has higher electrochemical activity associated with better electrochromic properties. In order to quantitatively compare the electrochromic performances of compact and porous WO_3 film, the transmittance spectra in colored and bleached states are measured under applied potential of –0.7 V and 1.0 V, respectively, as shown in Fig. 3b. The color of the WO_3 films changes from dark blue (colored state) to transparent (bleached state) reversibly. It can be seen that the porous WO_3 film exhibits an ultra large transmittance modulation reaching about 97.7% at 633 nm, the highest value for WO_3 so far, to the best of our knowledge,[12-14, 54-56] and it is much larger than that of the compact WO_3 film (61.5% at 633 nm). The digital photos of the porous WO_3 on bleached state and colored state are shown in inset of Fig. 3b. The coloration and bleaching speed of the WO_3 films are investigated by chronoamperometry (CA) and the corresponding in situ transmittance at 633 nm, as shown in Fig. 3c. The switching time is defined as the time required for a system to reach 90% of its full modulation. For the porous WO_3 film, the switching time for coloration and bleaching is 6 and 2.7 s respectively, which is comparable to the compact WO_3 film (6.9 and 1.9 s). However, the switching time of porous WO_3 film is much shorter than that of the compact WO_3 film to reach the same transmittance modulation. In comparison with many nanostructured WO_3 electrochromic materials, the switching speed of porous WO_3 reported in this work is much faster than that of WO_3 nanorolls (9 and 8 s),[57] WO_3 nanorods (272 and 364 s)[58] and WO_3 nanosheet (21 and 8 s)[59]. One of the most important criteria often used to characterize an electrochromic material is its coloration efficiency (CE). CE is defined as the change in optical density (ΔOD) per unit of charge (ΔQ) inserted into (or extracted from) the electrochromic layers. It can be calculated from the following formulas:[60]

$$CE(\lambda) = \frac{\Delta OD(\lambda)}{\Delta Q} \quad (5)$$

$$\Delta OD(\lambda) = \log \frac{T_b}{T_c} \quad (6)$$

where T_b and T_c refers to the transmittance in bleached and colored states, respectively. Generally, a high value of CE indicates that the electrochromic material exhibit a large optical modulation with a small intercalated (or extracted) charge density. The plots of OD at a wavelength of 633 nm as a function of inserted charge density at a potential of –0.7 V is shown in Fig. 3d, the CE can be calculated from the slope of the curves. The CE value is calculated to be 118 cm^2 C^{-1} at 633 nm for porous WO_3 film, which is higher than that of compact

WO_3 film. The CE value of 118 cm^2 C^{-1} is also higher than that of previous reported WO_3 nanomaterials, which istypically lower than 100 cm^2 C^{-1}.[61-63]

As we know, the optical modulation and the switching time of the electrochromic material are closely related to the applied potential. However, there are very few dedicated studies to this phenomenon. Fig. 4a shows the transmittance spectra of the porous WO_3 film as a function of applied potential. The transmittance spectra of the porous WO_3 film at 633 nm with respect to the applied potential is depicted in Table 1. It can be seen that the porous WO_3 film exhibits almost the same transmittance when the applied potential extends over 0.1 V, however, it is clear that the transmittance gradually decreases as the applied potential goes more negative. Meantime, the optical modulation gradually increases. Noticeably, our porous WO_3 film exhibits an optical modulation of about 82.9% at 633 nm by applying a narrow voltage window between 0.1~–0.4 V, and exhibits an optical modulation of about 93% at 633 nm by applying a voltage window between 0.1~–0.5 V. To the best of our knowledge, the new porous WO_3 film herein is among the best in documented inorganic materials. The switching time and the in situ transmittance at 633 nm were also recorded with respect to the applied potential as shown in Fig. 4b, c and Table 1. When the bleached potential is fixed as 0.3 V, the optical modulation gradually increases and colored switching time gradually decreases as the applied potential goes more negative. When the colored potential is fixed as –0.7 V, the film can fully beached only when the applied potential is over 0.1 V, and the beached switching time gradually decreases as the applied potential goes more positive. The results indicate that both large optical modulation and fast switching need applied wide voltage window. The electrochromic phenomenon of WO_3 is attributed to the injection/extraction of electrons and ions as shown in equation (4). The colored

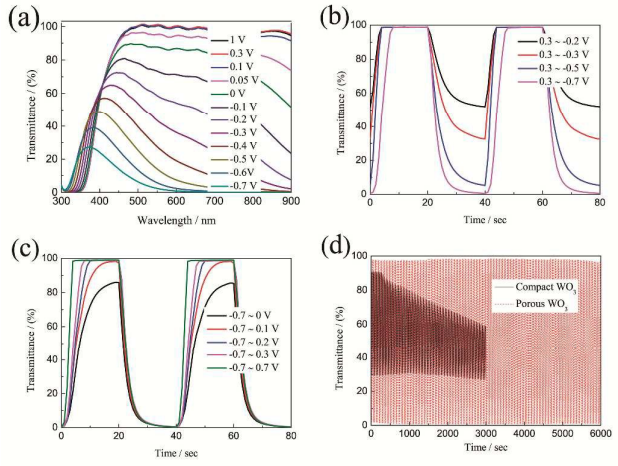

Fig.4 (a) Transmittance of porous WO_3 film as a function of applied potential. (b,c) In situ optical responses of porous WO_3 films measured at 633 nm as a function of applied potential. (d) Cycle performance of the WO_3 films measured in 0.5 M H_2SO_4 for 6000 s.

Table 1 Various parameters of porous WO_3 film as a function of applied potential.

Applied voltage (V)	Transmittance (%) at 633 nm	Applied voltage window	Switching time (s)
1.0	98.184	0.3~-0.2	t_c = 10.0
0.3	98.757	0.3~-0.3	t_c = 9.8
0.1	98.317	0.3~-0.5	t_c = 9.0
0.05	93.483	0.3~-0.7	t_c = 6.0
0	85.833	-0.7~0	t_b = 11.6
-0.1	70.173	-0.7~0.1	t_b = 10.2
-0.2	52.129	-0.7~0.2	t_b = 8.0
-0.3	32.76	-0.7~0.3	t_b = 6.5
-0.4	15.426	-0.7~0.7	t_b = 3.6
-0.5	5.222	-0.7~1.0	t_b = 2.7
-0.6	1.470	—	—
-0.7	0.495	—	—

and bleached processes correspond to the H^+ ion intercalated and extracted processes from the WO_3 material, respectively. Therefore, more negative potential applied on the film accompanied with insert of more H^+ into WO_3 material leads to reduction of W^{6+} ions to lower valence states and darker blue colour is observed till colour saturation, and vice versa. In addition, the larger potential means higher driven force for intercalation and extraction of H^+ ion which can improve the speed of the H^+ ion intercalation and extraction from the WO_3 material. Hence both large optical modulation and fast switching required a wider voltage window. Usually, the voltage window of –1.0~1.0 V is applied for WO_3 electrochromic material in H_2SO_4 or lithium perchlorate ($LiClO_4$) in propylene carbonate.[64-67] Wider voltage window will accelerate the dissolution of WO_3 dissolved in the electrolyte and affect the service life. Fig. 4d shows coloration–bleaching

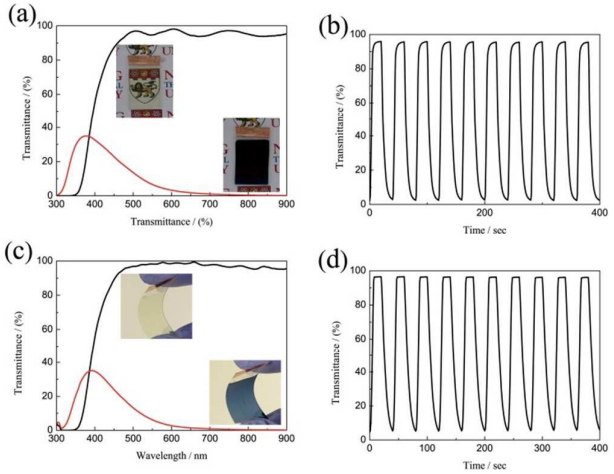

Fig.5 Transmittance spectra and in situ optical responses of the WO_3 films on different substrates between the colored and bleached states; (a,b) FTO substrate, (c,d) ITO–PET substrate.

cycles of the compact and porous WO_3 films by applying a voltage window switched between -0.7 V and 0.7 V with one cycle length for 20 s The test was conducted within 6000 s (300 switching cycles). The transmittance modulation of the compact WO_3 film gradually decreases during cycling process, and only sustains a transmittance modulation of about 52.4% of its initial value after subjected for 3000 s. While almost no change of the transmittance modulation of the porous WO_3 film was observed over the 6000 s. The stability of the porous WO_3 film is also better than that of the single–crystalline WO_3 quantum dots[13] and thiourea-assisted prepared nanostructured WO_3[68], in which the degradation was observed just after 50 repeated switching cycles. These results indicate that the porous WO_3 film possesses reasonably good cycling durability. The improved electrochromic properties of the porous WO_3 film are mainly attributed to the porous structure, which facilitates the charge-transfer and alleviates the expansion of the WO_3 material during H^+ insertion.[69-71] To further understand the electrochemical behavior of the compact and porous WO_3 films, a nondestructive and sensitive technique, EIS, is conducted in a frequency range of 100 kHz to 0.1 Hz at open-circuited potential. Fig. S5 shows the Nyquist plots of the compact and porous WO_3 films, the intercept at the real axis (Z') contains the intrinsic resistance of the substrate, electrolyte resistance, and the contact resistance between active material and substrate. In addition, both EIS spectra consist of a semicircle in high-frequency region and a straight line in low frequency region. The semicircle is related to the charge transfer impedance, the straight line is ascribed to the diffusion-controlled Warburg impedance.[72-75] Obviously, the porous WO_3 film exhibits a lower intercept at the real axis and a smaller semicircle in the high frequency region, indicating smaller contact resistance and charger transfer resistance compared to that of the compact WO_3 film.

The large optical modulation and fast switching speed of the porous WO_3 were not only observed on the ITO substrate, but could also be achieved on FTO–coated glass and ITO–coated PET flexible substrate as shown in Fig. 5. The porous WO_3 films deposited on FTO glass and ITO–coated PET flexible substrate exhibit an optical modulation of 93.8% and 96.6% at 633 nm, respectively. The colored/bleached switching time of the WO_3 deposited on FTO glass and ITO–coated PET flexible substrate are 9.2/4.6 and 14/6.6 s, respectively. The digital photos of the porous WO_3 on bleached state and colored state are shown in corresponding inset of Fig. 5a and 5c. The results indicated the good electrochromic performance can obtained on various transparent conductive substrates.

3.3 Local visualization of redox activity by SECM

In order to further understand the relationships between structural and electrochemical activity of the electrochromic material, local electrochemistry of the electrode materials was studied using SECM. SECM has been considered as an essential tool to study not only the local electrochemical activity of the surface at micrometric scales, but also to evaluate local topographical characteristics of the scanned area. In the typical SECM measurement, the localized CVs of WE1 were carried out in the bulk of mediator solution $[Ru(NH_3)_6]^{3+}/[Ru(NH_3)_6]^{2+}$ as well as near to the WE2 surface. Fig. S6a and c show localized CVs of WE1 on the surface of compact and porous WO_3 films, respectively, at a calibrated distance of ~200 µm and ~2.5 µm from the surface of WE2. It is evident from the CV analysis that the tip current at the surface of porous WO_3 film is slightly higher than that of the compact WO_3 film, which indicates its higher amount of regeneration of redox mediator species which in turns improve the tip current. To gain insight on the mechanism of this regeneration, approach curve analyses were performed. In the approach curve analysis, a constant potential of –0.3 V was applied to the WE1, while the WE2 (WO_3 films) was unbiased. The approach curve analyses in terms of normalized tip current vs. normalized distance on the surface of compact and porous WO_3(Fig. S6 b and d), respectively, reveal that both the samples show positive feedback behavior. Notably, the effective heterogeneous charge transfer rate constants of local regeneration of redox mediator ($[Ru(NH_3)_6]^{2+}/[Ru(NH_3)_6]^{3+}$) on the surface of porous WO_3 film (k_{eff}=3.49 × 10^{-2} cm s^{-1} which is calculated in Supporting Information) is found slightly higher than that of the compact deposited WO_3 film (k_{eff}=2.63 × 10^{-2} cm s^{-1}). The origin of this improvement may be due to the microstructural features of the porous WO_3 film. To examine the effect of microstructural features on the rate of

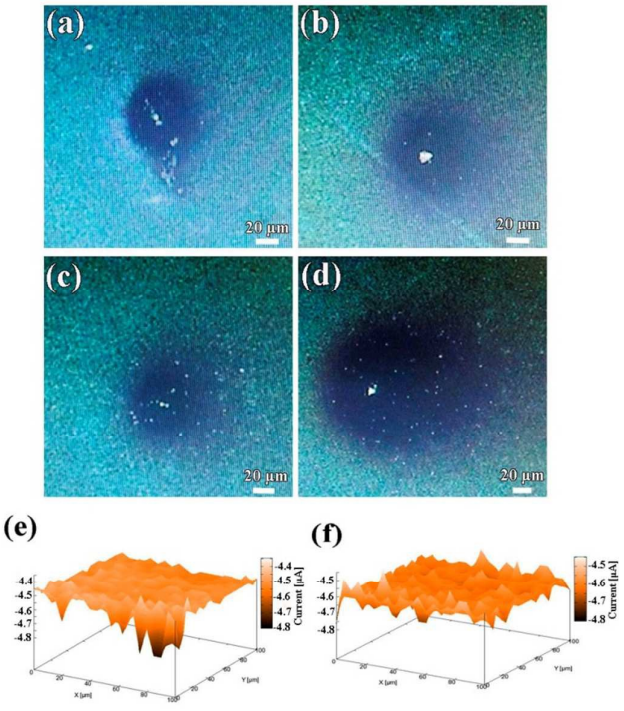

Fig.6 Optical micrographs of the WO_3 in the surrounding of $[Ru(NH_3)_6]^{2+}/[Ru(NH_3)_6]^{3+}$ redox mediator for 2 and 15 mins: (a,b) compact WO_3 film, (c,d) porous WO_3 film. Electrochemical mappings of (e) compact WO_3 film, (f) porous WO_3 film.

regeneration or propagation of redox mediator species, delayed time analysis were performed by positioning the WE1 (fixed at a distance of about 5 μm and at–0.3 V) near to the surface of compact and porous WO_3 film for 2 min and 15 min, as shown in Fig. 6a, b and c, d, respectively. The rate of propagation (μm s^{-1}) of the charged species in porous WO_3 film (~0.25 μm s^{-1} to ~0.75 μm s^{-1}) is found much faster than that of the compact WO_3 film (~0.25 μm s^{-1} to ~0.5 μm s^{-1}), in the given time domain. To further investigate the local electrochemical activity of the as–deposited WO_3 films, current maps measurements were conducted. Fig. 6e and f display the three–dimensional spatial resolution of the local tip currents obtained in the "comb–like" mode of SECM at a constant height of about 10 μm with a translational speed of 2 μm s^{-1} and keeping WE1 at a constant potential of –0.3 V by rastering the tip over a 100 × 100 μm^2 region of the WO_3 films. Both vertical and color scales reflect the magnitude of the currents measured by the SECM probe as it was scanned above the WO_3 films. Except some small zone, the current response of compact WO_3 film over the whole surface is almost smooth and constant around –4.45 nA, indicating uniform activity across the electrode surface (Fig. 6e). However, the current response of porous WO_3 is in noticeable contrast as shown in Fig. 6f. The area imaged over the porous WO_3 film shows tip collection currents extremely rough and the most tip collection current reached to –4.60 nA, which exhibits higher activity than that of the compact WO_3 film. In addition, the higher current response of the porous WO_3 film is correlated to its structure and leads to higher surface reactivity, which in turn accountable for its better electrochromic performances than that of compact WO_3 film.

Conclusions

The present work demonstrates the best transmittance modulation exhibited by porous WO_3 film which was successfully fabricated on different substrates by a facile, scalable and economical pulsed electrochemical deposited method with 1.1 s interval time between each pulse. The porous WO_3 exhibits highly enhanced ion insertion and electrochromic properties with near theory optical modulation, fast switching speed, high coloration efficiency, and excellent cycling stability. Compared with the compact WO_3, the porous WO_3 exhibits such outstanding electrochromic performance mainly due to porous structure, which not only makes the charge-transfer and the electrolyte penetration becomes easier within the film, but also alleviates the expansion of the WO_3 during H^+ insertion and extraction. In addition, the relationships between structural and electrochemical activity of the electrochromic material were further systematic studied by the SECM. These results testify that the porous structure can promote the infiltration of electrolyte and reduce the diffuse path, and consequently speed up the electrochemical activity.

Acknowledgements

This research is supported by A*Star–MND Green Building Joint Grant 1321760013. Part of the work is also supported by NTU–HUJ–BGU Nanomaterials for Energy and Water Management Programme under the Campus for Research Excellence and Technological Enterprise (CREATE) and the National Research Foundation Competitive Research Programme, Award No. NRF-CRP–13–2014–02, that is supported by the National Research Foundation, Prime Minister's Office, Singapore..

Notes and references

1 P. Simon and Y. Gogotsi, *Nat. Mater.*, 2008, **7**, 845-854.
2 V. Engelhardt, S. Kuhri, J. Fleischhauer, M. Garcia-Iglesias, D. Gonzalez-Rodriguez, G. Bottari, T. Torres, D. M. Guldi and R. Faust, *Chemical Science*, 2013, **4**, 3888-3893.
3 X. H. Yang, G. Zhu, S. H. Wang, R. Zhang, L. Lin, W. Z. Wu and Z. L. Wang, *Energy Environ. Sci.*, 2012, 5, 9462-9466.
4 C. G. Granqvist, *Sol. Energy Mater. Sol. Cells*, 2012, **99**, 1-13.
5 M. Gratzel, *Nature*, 2001, **409**, 575-576.
6 C. G. Granqvist, *Thin Solid Films*, 2014, **564**, 1-38.
7 G. F. Cai, X. Wang, M. Q. Cui, P. Darmawan, J. X. Wang, A. L.-S. Eh and P. S. Lee, *Nano Energy*, 2015, **12**, 258-267.
8 C. Park, S. Seo, H. Shin, B. D. Sarwade, J. Na and E. Kim, *Chemical Science*, 2015, **6**, 596-602.
9 K. Wang, H. P. Wu, Y. N. Meng, Y. J. Zhang and Z. X. Wei, *Energy Environ. Sci.*, 2012, **5**, 8384-8389.
10 G. A. Niklasson and C. G. Granqvist, *J. Mater. Chem.*, 2007, **17**, 127-156.
11 C. G. Granqvist, *Sol. Energy Mater. Sol. Cells*, 2000, **60**, 201-262.
12 P. H. Yang, P. Sun, Z. S. Chai, L. H. Huang, X. Cai, S. Z. Tan, J. H. Song and W. J. Mai, *Angew. Chem. Int. Ed.*, 2014, **53**, 11935-11939.
13 S. Cong, Y. Y. Tian, Q. W. Li, Z. G. Zhao and F. X. Geng, *Adv. Mater.*, 2014, **26**, 4260-4267.
14 L. Liu, M. Layani, S. Yellinek, A. Kamyshny, H. Ling, P. S. Lee, S. Magdassi and D. Mandler, *J. Mater. Chem. A*, 2014, **2**, 16224-16229.
15 R.-T. Wen, C. G. Granqvist and G. A. Niklasson, *Nat. Mater.*, 2015, **14**, 996–1001.
16 Z. H. Jiao, X. Wang, J. M. Wang, L. Ke, H. V. Demir, T. W. Koh and X. W. Sun, *Chem. Commun.*, 2012, **48**, 365-367.
17 F. Lin, J. Cheng, C. Engtrakul, A. C. Dillon, D. Nordlund, R. G. Moore, T.-C. Weng, S. K. R. Williams and R. M. Richards, *J. Mater. Chem.*, 2012, **22**, 16817-16823.
18 J. Thangala, S. Vaddiraju, R. Bogale, R. Thurman, T. Powers, B. Deb and M. K. Sunkara, *Small*, 2007, **3**, 890-896.
19 N. Naseri, R. Azimirad, O. Akhavan and A. Z. Moshfegh, *Thin Solid Films*, 2010, **518**, 2250-2257.
20 J. Zhang, X. L. Wang, X. H. Xia, C. D. Gu, Z. J. Zhao and J. P. Tu, *Electrochim. Acta*, 2010, **55**, 6953-6958.
21 J. Zhang, J. P. Tu, X. H. Xia, X. L. Wang and C. D. Gu, *J. Mater. Chem.*, 2011, **21**, 5492-5498.
22 G. F. Cai, J. P. Tu, D. Zhou, X. L. Wang and C. D. Gu, *Sol. Energy Mater. Sol. Cells*, 2014, **124**, 103-110.
23 J. Z. Ou, S. Balendhran, M. R. Field, D. G. McCulloch, A. S. Zoolfakar, R. A. Rani, S. Zhuiykov, A. P. O'Mullane and K. Kalantar-zadeh, *Nanoscale*, 2012, **4**, 5980-5988.
24 Z. B. Cai, L. Li, J. Ren, L. B. Qiu, H. J. Lin and H. S. Peng, *J. Mater. Chem. A*, 2013, **1**, 258-261.
25 C. Y. Yan and P. S. Lee, *Small*, 2014, **10**, 3443-3460.
26 C. Y. Yan, W. B. Kang, J. X. Wang, M. Q. Cui, X. Wang, C. Y. Foo, K. J. Chee and P. S. Lee, *ACS Nano*, 2013, **8**, 316-322.
27 T. Pauporté, *J. Electrochem. Soc.*, 2002, 149, C539-C545.

28 Z. R. Yu, X. D. Jia, J. H. Du and J. Y. Zhang, *Sol. Energy Mater. Sol. Cells*, 2000, **64**, 55-63.
29 S. H. Baeck, T. Jaramillo, G. D. Stucky and E. W. McFarland, *Nano Lett.*, 2002, 2, 831-834.
30 I. Turyan, B. Orel, R. Reisfeld and D. Mandler, *PCCP*, 2003, **5**, 3212-3219.
31 I. Turyan, U. O. Krasovec, B. Orel, T. Saraidorov, R. Reisfeld and D. Mandler, *Adv. Mater.*, 2000, **12**, 330-333.
32 S. V. Kalinin and N. Balke, *Adv. Mater.*, 2010, 22, E193-E209.
33 M. Arca, M. V. Mirkin and A. J. Bard, *The Journal of Physical Chemistry*, 1995, **99**, 5040-5050.
34 A. Sumboja, U. M. Tefashe, G. Wittstock and P. S. Lee, *J. Power Sources*, 2012, **207**, 205-211.
35 A. Sumboja, U. M. Tefashe, G. Wittstock and P. S. Lee, *Adv. Mater. Interfaces*, 2015, **2**,1400154.
36 R. Cornut and C. Lefrou, *J. Electroanal. Chem.*, 2008, **621**, 178-184.
37 Y. Kazusuke, O. Hiroshi, K. Hirokazu and K. Tetsuichi, *Jpn. J. Appl. Phys.*, 1986, **25**, 1420-1426.
38 C.-X. Qi, Z. Tan, Z.-H. Feng and L.-P. Yu, *J. Mater. Sci. Mater. Electron.*, 2014, **25**, 1553-1558.
39 V. A. Gritsenko, Y. O. Roisin, L. E. Semenchuk and N. L. Schwarz, *Solid State Commun.*, 1981, **38**, 351-352.
40 S. H. Park, H. S. Shin, Y. H. Kim, H. M. Park and J. Y. Song, *Nanoscale*, 2013, **5**, 1864-1869.
41 Y. Sawada, A. Dougherty and J. Gollub, *Phys. Rev. Lett.*, 1986, **56**, 1260-1263.
42 D. Chatzikyriakou, N. Krins, B. Gilbert, P. Colson, J. Dewalque, J. Denayer, R. Cloots and C. Henrist, *Electrochim. Acta*, 2014, **137**, 75-82.
43 Y. Djaoued, S. Priya and S. Balaji, *J. Non-Cryst. Solids*, 2008, **354**, 673-679.
44 M. F. Daniel, B. Desbat, J. C. Lassegues, B. Gerand and M. Figlarz, *J. Solid State Chem.*, 1987, **67**, 235-247.
45 W. Chun-Kai, D. R. Sahu, W. Sheng-Chang, L. Chung-Kwei and H. Jow-Lay, *J. Phys. D: Appl. Phys.*, 2012, **45**, 225303.
46 G. F. Cai, D. Zhou, Q. Q. Xiong, J. H. Zhang, X. L. Wang, C. D. Gu and J. P. Tu, *Sol. Energy Mater. Sol. Cells*, 2013, **117**, 231-238.
47 J. Zhang, J. P. Tu, G. F. Cai, G. H. Du, X. L. Wang and P. C. Liu, *Electrochim. Acta*, 2013, **99**, 1-8.
48 L. L. Yang, D. T. Ge, J. P. Zhao, Y. B. Ding, X. P. Kong and Y. Li, *Sol. Energy Mater. Sol. Cells*, 2012, **100**, 251-257.
49 H.-C. Lin, C.-Y. Su, Y.-H. Yu and C.-K. Lin, *J. Nanopart. Res.*, 2012, **14**, 1-10.
50 G. F. Cai, X. L. Wang, D. Zhou, J. H. Zhang, Q. Q. Xiong, C. D. Gu and J. P. Tu, *Rsc Advances*, 2013, **3**, 6896-6905.
51 S. H. Lee, R. Deshpande, P. A. Parilla, K. M. Jones, B. To, A. H. Mahan and A. C. Dillon, *Adv. Mater.*, 2006, **18**, 763-766.
52 A. Llordes, G. Garcia, J. Gazquez and D. J. Milliron, *Nature*, 2013, **500**, 323-326.
53 M. Rezrazi, O. Bohnke and J. Pagetti, *Displays*, 1987, **8**, 119-126.
54 J. Denayer, P. Aubry, G. Bister, G. Spronck, P. Colson, B. Vertruyen, V. Lardot, F. Cambier, C. Henrist and R. Cloots, *Sol. Energy Mater. Sol. Cells*, 2014, **130**, 623-628.
55 M. Layani, P. Darmawan, W. L. Foo, L. Liu, A. Kamyshny, D. Mandler, S. Magdassi and P. S. Lee, *Nanoscale*, 2014, **6**, 4572-4576.
56 G. F. Cai, J. P. Tu, D. Zhou, L. Li, J. H. Zhang, X. L. Wang and C. D. Gu, *CrystEngComm*, 2014, **16**, 6866-6872.
57 S. Vankova, S. Zanarini, J. Amici, F. Camara, R. Arletti, S. Bodoardo and N. Penazzi, *Nanoscale*, 2015, **7**, 7174-7177.
58 J. M. Wang, E. Khoo, P. S. Lee and J. Ma, *J. Phys. Chem. C*, 2008, **112**, 14306-14312.
59 H. Z. Li, J. M. Wang, G. Y. Shi, H. Z. Wang, Q. H. Zhang and Y. G. Li, *RSC Advances*, 2015, **5**, 196-201.
60 L. C. Chen and K. C. Ho, *Electrochim. Acta*, 2001, **46**, 2151-2158.
61 C. P. Fu, C. Y. Foo and P. S. Lee, Electrochim. Acta, 2014, **117**, 139-144.
62 R. Giannuzzi, M. Balandeh, A. Mezzetti, L. Meda, P. Pattathil, G. Gigli, F. Di Fonzo and M. Manca, Adv. Opt. Mater., 2015, DOI: 10.1002/adom.201500152.
63 C. Y. Ng, K. Abdul Razak and Z. Lockman, Electrochim. Acta, 2015, **178**, 673-681.
64 J. M. Wang, E. Khoo, P. S. Lee and J. Ma, *J. Phys. Chem. C*, 2009, **113**, 9655-9658.
65 W. Xiao, W. T. Liu, X. H. Mao, H. Zhu and D. H. Wang, *J. Mater. Chem. A*, 2013, **1**, 1261-1269.
66 J.-W. Liu, J. Zheng, J.-L. Wang, J. Xu, H.-H. Li and S.-H. Yu, *Nano Lett.*, 2013, **13**, 3589-3593.
67 H. Z. Li, G. Y. Shi, H. Z. Wang, Q. H. Zhang and Y. G. Li, *J. Mater. Chem. A*, 2014, **2**, 11305-11310.
68 W.-T. Wu, W.-P. Liao, J.-S. Chen and J.-J. Wu, *Chemphyschem*, 2010, **11**, 3306-3312.
69 M. Q. Cui, W. S. Ng, X. Wang, P. Darmawan and P. S. Lee, *Adv. Funct. Mater.*, 2015, **25**, 401-408.
70 W. B. Kang, C. Y. Yan, X. Wang, C. Y. Foo, A. W. Ming Tan, K. J. Zhi Chee and P. S. Lee, *J. Mater. Chem. C*, 2014, **2**, 4727-4732.
71 T. Brezesinski, D. Fattakhova Rohlfing, S. Sallard, M. Antonietti and B. M. Smarsly, *Small*, 2006, **2**, 1203-1211.
72 J. A. Lee, M. K. Shin, S. H. Kim, H. U. Cho, G. M. Spinks, G. G. Wallace, M. D. Lima, X. Lepró, M. E. Kozlov, R. H. Baughman and S. J. Kim, *Nat Commun*, 2013, 4, 1970.
73 X. Wang, W. S. Liu, X. Lu and P. S. Lee, *J. Mater. Chem.*, 2012, **22**, 23114-23119.
74 L. B. Liu, Y. Yu, C. Yan, K. Li and Z. J. Zheng, *Nat Commun*, 2015, **6**, 7260.
75 Y. M. He, W. J. Chen, X. D. Li, Z. X. Zhang, J. C. Fu, C. H. Zhao and E. Q. Xie, *ACS Nano*, 2013, **7**, 174-182.